


**Pressure-induced superconductivity in the kagome single-crystal Pd<sub>3</sub>P<sub>2</sub>S<sub>8</sub>**Ying Zhou <sup>1</sup>, Xinyi He,<sup>1</sup> Shuyang Wang,<sup>2,3</sup> Jing Wang,<sup>2,3</sup> Xuliang Chen,<sup>2,3</sup> Yonghui Zhou,<sup>2,3</sup> Chao An,<sup>1</sup> Min Zhang,<sup>1</sup> Zhitao Zhang <sup>2,3,\*</sup> and Zhaorong Yang<sup>1,2,3,†</sup><sup>1</sup>*Institutes of Physical Science and Information Technology, Anhui University, Hefei 230601, China*<sup>2</sup>*Anhui Province Key Laboratory of Condensed Matter Physics at Extreme Conditions, High Magnetic Field Laboratory, HFIPS, Chinese Academy of Sciences, Hefei 230031, China*<sup>3</sup>*High Magnetic Field Laboratory of Anhui Province, Hefei 230031, China*

(Received 6 April 2022; accepted 31 August 2022; published 20 September 2022)

The kagome lattice offers unique opportunities for the exploration of unusual quantum states of correlated electrons. Here, we report on the observation of superconductivity in a kagome single-crystal Pd<sub>3</sub>P<sub>2</sub>S<sub>8</sub> when a semiconducting-to-metallic transition is driven by pressure. High-pressure resistance measurements show that the metallization and superconductivity are simultaneously observed at about 11 GPa. With increasing pressure, the superconducting critical temperature  $T_c$  is monotonously enhanced from 2.6 K to a maximum 7.7 K at  $\sim 52$  GPa. Interestingly, superconductivity is retained when the pressure is fully released. Synchrotron x-ray diffraction and Raman experiments consistently evidence that the emergence of superconductivity is accompanied with an amorphization, and the retainability of superconductivity upon decompression can be attributed to the irreversibility of the amorphization.

DOI: [10.1103/PhysRevB.106.104512](https://doi.org/10.1103/PhysRevB.106.104512)**I. INTRODUCTION**

Generally, the geometrically frustrated kagome lattice is expected to have both flat-band and Dirac dispersion bands, where the former can promote the electron correlations through destructive interference-induced localization [1,2]. With the presence of the peculiar electronic structure and strong correlation effects, kagome materials often exhibit various and highly tunable electronic instabilities, including the spin liquid state, anomalous Hall effect, unconventional superconductivity, and so on [3–8]. Particularly, flat-band systems are considered ideal platforms to explore for exotic superconductivity [9–14]. For example, theoretical studies proposed that high-critical temperature ( $T_c$ ) superconductivity could be realized in flat-band systems through utilizing the interband pair scatterings between dispersion bands and the flatband, which has divergent density of states [9–11].

Pd<sub>3</sub>P<sub>2</sub>S<sub>8</sub> is a two-dimensional kagome semiconductor that so far is mainly utilized as nanomaterials for photodetection, sensing, catalyzing, etc. [15–19]. Recently, DFT calculations demonstrated that Pd<sub>3</sub>P<sub>2</sub>S<sub>8</sub> has a flat band located right below the Fermi level, which is primarily from Pd  $4d$ -orbitals [20,21]. Therefore, it would be of particular interest to explore for superconductivity in Pd<sub>3</sub>P<sub>2</sub>S<sub>8</sub> if a metallization transition can be induced, for example, by element doping or pressure. Yan *et al.* [20] showed that Se substitution for S atoms is able to reduce the band gap to some extent. However, the solubility limit of Se substitution (<25%) prevents a potentially existing metallization from taking place [20].

We grew high-quality Pd<sub>3</sub>P<sub>2</sub>S<sub>8</sub> single crystals and performed comprehensive high-pressure electrical resistance, Raman, and x-ray diffraction (XRD) measurements to investigate the pressure evolution of electronic properties and to search for superconductivity in the kagome system Pd<sub>3</sub>P<sub>2</sub>S<sub>8</sub>. At a critical pressure of about 11 GPa, we observe concurrence of metallization and superconductivity with a  $T_c$  of 2.6 K. The superconductivity is continuously enhanced by further compression and survives after the pressure is reduced to ambient pressure. Based on structural analyses, we find that the occurrence of superconductivity and its retainability upon decompression are directly related to an irreversible amorphization process.

**II. EXPERIMENTAL METHODS**

Pd<sub>3</sub>P<sub>2</sub>S<sub>8</sub> single crystals were synthesized via a chemical vapor transport method with iodine as a transport agent [21]. The phase purity of the samples was determined by XRD measurements on single crystals and powdered crystals. Stoichiometry of the crystals was confirmed by energy dispersive x-ray spectrometry (EDXS) with area- and point-scanning modes. Optical transmittance absorption spectra were collected by using a UV/visible/near-infrared spectrometer. High-pressure electrical transport experiments were performed in a nonmagnetic Be-Cu diamond-anvil cell using an in-house 9-T transport property measurement system [22]. High-pressure Raman scattering and angle-dispersive synchrotron XRD measurements were conducted in a Mao-Bell cell with Daphne 7373 as the transmitting medium. The Raman spectra were recorded with cleaved single-crystal flakes using a commercial Renishaw spectroscopy system with a 532-nm laser excitation line. Synchrotron XRD

\* ztzhang@hmf.ac.cn

† zryang@issp.ac.cn

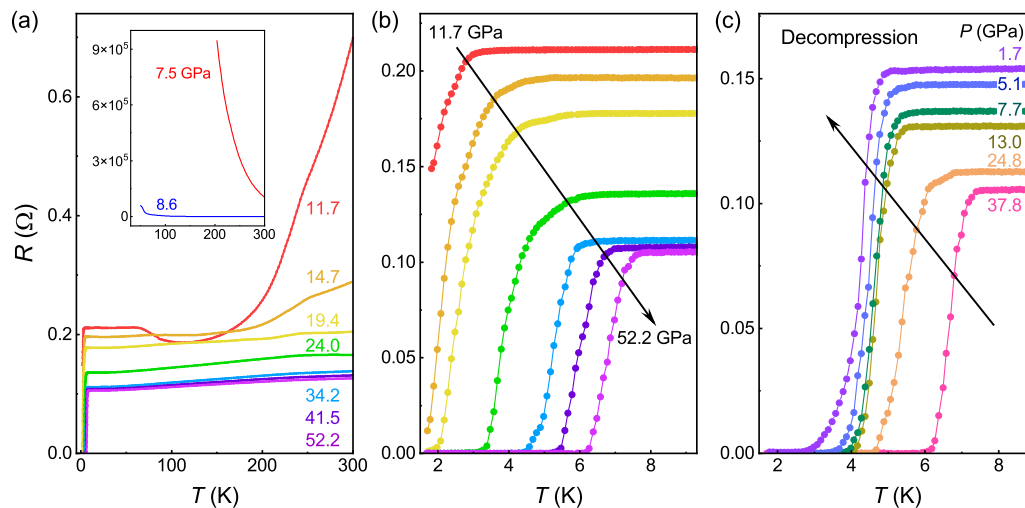


FIG. 1. (a) Temperature-dependent resistance curves  $R(T)$  for the  $\text{Pd}_3\text{P}_2\text{S}_8$  single crystal measured at different pressures. The inset displays the curves for low pressures of 7.5 GPa and 8.6 GPa. (b) A zoomed-in view of the  $R(T)$  curves near the superconducting critical temperatures. (c) The  $R(T)$  curves upon decompression from 37.8 GPa to 1.7 GPa.

experiments were performed with powdered crystals at the beamline BL15U1 of Shanghai Synchrotron Radiation Facility. Pressure was applied at room temperature and calibrated by using the ruby fluorescence shifts for all experiments [23].

### III. RESULTS AND DISCUSSION

The crystal structure, phase purity, chemical composition, and band gap of the as-grown  $\text{Pd}_3\text{P}_2\text{S}_8$  single crystals were examined by XRD, Raman, EDXS, and optical transmittance measurements, for which the results are presented in Supplemental Material Figs. S1 and S2 [24]. Based on a comparison with previous reports on  $\text{Pd}_3\text{P}_2\text{S}_8$  single crystals, all the results consistently indicate a high quality of the single crystals [24]. The actual chemical composition of the single crystals determined by the EDXS analysis is  $\text{Pd}_{3.12\pm 0.03}\text{P}_{2.22\pm 0.03}\text{S}_8$ , which is close to the stoichiometric  $\text{Pd}_3\text{P}_2\text{S}_8$  [24].

High-pressure resistance measurements were performed on a  $\text{Pd}_3\text{P}_2\text{S}_8$  single crystal for investigating the pressure evolution of the electronic ground state. Due to the limited measuring range of the instrument, resistance measurements are only available for pressures more than 7.5 GPa, given that  $\text{Pd}_3\text{P}_2\text{S}_8$  at ambient pressure is a semiconductor with a large band gap of 1.9 to 2.1 eV [20,21]. Figure 1(a) presents the temperature-dependent resistance curves  $R(T)$  for the single crystal measured at different pressures. At low pressures of 7.5 to 8.6 GPa, the  $R(T)$  curves exhibit semiconducting behaviors. Meanwhile, the amplitude of resistance is dramatically suppressed with increasing pressure. From 11.7 GPa to above, however, a metallic behavior is instead observed. Upon entering the metallic phase, a sharp resistance drop is observed at an onset temperature of 2.6 K, as shown in Fig. 1(b). When pressure is raised up to 19.4 GPa, a zero-resistance state is probed at 1.8 K, indicating the presence of superconductivity. Both the onset superconducting critical temperature  $T_c^{\text{onset}}$  and zero-resistance temperature  $T_c^{\text{zero}}$  display monotonous increases with increasing pressure to 52.2 GPa. Upon decompression [see Fig. 1(c)], we find that the superconductivity can be preserved to an ambient condition, though both  $T_c^{\text{onset}}$  and

$T_c^{\text{zero}}$  are slightly reduced. In order to confirm the observation of pressure-induced superconductivity, a second run (Run 2) of transport measurements was carried out (see Supplemental Material Fig. S3 [24]). In Run 2, the pressure-induced superconductivity as well as the concomitant insulating-to-metallic transition was reproducible, although at a slightly higher pressure.

Figure 2(a) presents the evolution of superconductivity against a magnetic field, which is measured at the highest pressure (52.2 GPa). As expected, superconductivity is gradually suppressed with increasing magnetic field. In Fig. 2(b), we summarize the extracted upper critical field  $\mu_0 H_{c2}$  as a function of critical temperature  $T_c^{90\%}$ , which is defined by the temperature where the normal-state resistance drops by 10%. By fitting the data to the Werthamer–Helfand–Hohenberg (WHH) model [27], we obtain a zero-temperature limit of the upper critical field  $\mu_0 H_{c2}(0)$  of 6.15 T.

In order to find out the underlying structural evolution during the development of superconductivity, we performed

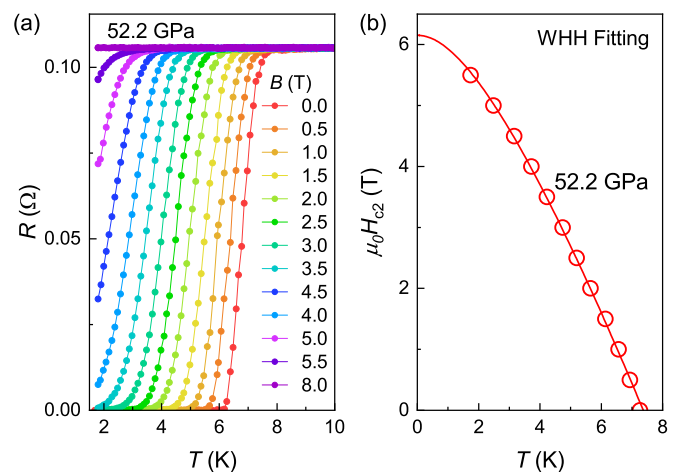


FIG. 2. (a) Magnetic-field evolution of superconducting resistive transition measured at pressure 52.2 GPa. (b) The upper critical field  $\mu_0 H_{c2}(T)$  as a function of superconducting critical temperature  $T_c^{90\%}$ .

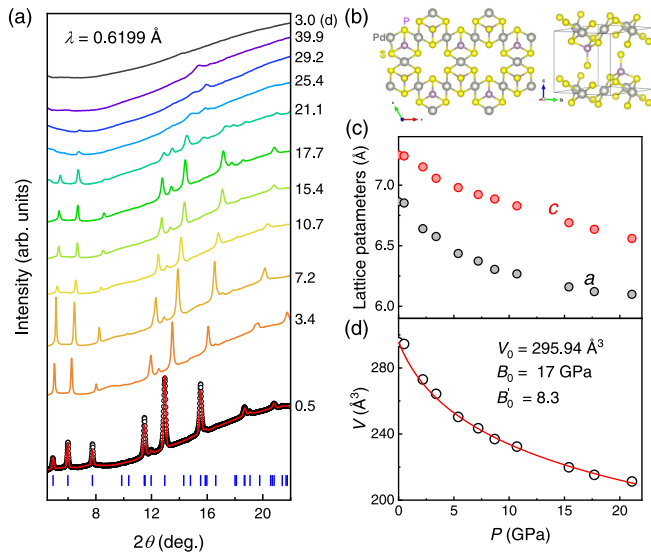


FIG. 3. (a) High-pressure powder XRD patterns measured on grounded  $\text{Pd}_3\text{P}_2\text{S}_8$  crystals for pressures up to 39.9 GPa, and then down to 3.0 GPa (“d” means decompression). For  $P = 0.5$  GPa, a red solid line presents a representative fitting. (b) Crystal structure of  $\text{Pd}_3\text{P}_2\text{S}_8$  from a top view and side view, where the kagome lattice of Pd atoms is clearly shown. (c) Pressure dependences of the fitted lattice parameters  $a$  and  $c$ . (d) Pressure dependence of the unit-cell volume  $V$ . The red solid line represents a fitting to the data using the third-order Birch–Murnaghan equation of states.

angle-dispersive synchrotron XRD experiments on powdered crystals of  $\text{Pd}_3\text{P}_2\text{S}_8$ , for which the results are given in Fig. 3(a). For the initial pressure 0.5 GPa, all the diffraction peaks can be well indexed and fitted by the space group  $P-3m1$  (No. 164), which is the same as that at ambient pressure, as is schematically shown in Fig. 3(b). Below 21.1 GPa, no new diffraction peak appears, indicating the absence of any structural transition. Above 21.1 GPa, however, most of the diffraction peaks rapidly disappear, with the exception of a remaining weak peak at  $\sim 15.3^\circ$  at 39.9 GPa, which is associated with a lanthanum gasket. The results fully agree with those in a recent similar work [28]. In addition, the peaks are broadened before disappearing (Supplemental Material Fig. S5 [24]). The concomitant broadening and disappearance of the XRD peaks may originate from a pressure-induced amorphization. Although a possible reduction in the particle size can also cause peak broadening, it does not result in the disappearance of the diffraction peaks [29,30]. When pressure is released to 3.0 GPa, none of the crystalline diffraction peaks is restored. The irreversible evolution of structure is consistent with the irreversible development of superconductivity, as is presented by the transport measurements. The difference of transition pressure between XRD and the transport measurements can be attributed to the distinct pressure-transmitting media and the different sensitivities between the probing techniques. Moreover, the wait time given for equilibration at each pressure should not be a main factor, because a typical timescale of solid-state transformations under static high pressures ranges from microseconds to milliseconds [31,32], whereas the wait time in the present work is as long as 5 to

10 minutes for XRD measurements and 5 to 24 hours for the transport measurements.

The lattice parameters  $a$ ,  $c$ , and unit-cell volume  $V$  are extracted by fittings and plotted as functions of pressure in Fig. 3(c) and 3(d). All these parameters monotonously decrease with pressure. Isothermal equations of state were fitted on the unit-cell volume  $V$  by using the third-order Birch–Murnaghan formula [33]:  $P = \frac{3}{2}B_0[(\frac{V_0}{V})^{\frac{7}{3}} - (\frac{V_0}{V})^{\frac{5}{3}}][1 + \frac{3}{4}(B'_0 - 4)[(\frac{V_0}{V})^{\frac{2}{3}} - 1]]$ , where  $V_0$ ,  $B_0$ , and  $B'_0$  are volume, bulk modulus  $-V/(dV/dP)$ , and the first-order derivative of the bulk modulus at ambient pressure, respectively. With  $V_0$  fixed as  $295.94 \text{ \AA}^3$ , our fitting yields  $B_0 = 17 \text{ GPa}$ , and  $B'_0 = 8.3$ .

The high-pressure structure of the  $\text{Pd}_3\text{P}_2\text{S}_8$  single crystal is further examined by Raman experiments. During the measurements, we incidentally collected the optical micrographs for the single crystal, which are shown in Fig. 4(a). From 1.2 GPa to 10.4 GPa, the single crystal is partially transparent and becomes darker and darker with increasing pressure, which corresponds to a gradually increased reflection of visible light due to the increment of charge carrier concentration. For pressures above 11.8 GPa, the sample becomes totally black, characterizing a metallic nature of the sample. After decompression to 0.5 GPa, the black color remains, which agrees with the irreversible evolution of the transport properties.

Figure 4(b) presents the Raman spectra of the  $\text{Pd}_3\text{P}_2\text{S}_8$  single crystal measured at different pressures. At 0.2 GPa, all the present Raman modes are consistent with those measured at ambient pressure [15,24,25]. With increasing pressure, the Raman spectral intensity exhibits a decline at 10.4 GPa, and all Raman modes finally disappear above 17.9 GPa. Generally, the disappearance of Raman peaks may originate from reasons such as (i) structural disorder, (ii) an insulator–metal transition, and/or (iii) adoption of a high-symmetry Raman-inactive phase [34]. In the present work, the disappearance of Raman peaks for  $\text{Pd}_3\text{P}_2\text{S}_8$  above 17.9 GPa should be ascribed to both effects of the pressure-induced amorphization and the insulator–metal transition. The pressure of 17.9 GPa is slightly lower than that of 21.1 GPa in the XRD measurements where the diffraction peaks disappear. Such a difference might originate from the following two reasons: first, Raman spectroscopy probes more local-range order compared to XRD [35]; second, besides being dependent on the variation of structure, the signal intensity of Raman spectra should also be sensitive to the increase of charge carrier density when the system is going through a metallization, because the Raman cross section is reduced due to the screening of the charge by the longitudinal electric field [36,37]. When pressure is released down to 0.5 GPa, no Raman mode is stored, consistent with the irreversible evolution of the XRD pattern.

The frequencies of the Raman modes are extracted and plotted as functions of pressure in Fig. 4(c). The smooth evolutions of the mode frequencies, in combination with the fact that no new Raman mode is present, evidence that no structural transition takes place below 17.9 GPa, which is in line with the XRD results. While most of the Raman modes expectedly show blueshifts with increasing pressure, only the modes  $E_g^1$  and  $E_g^2$  exhibit unusual redshifts. Generally,

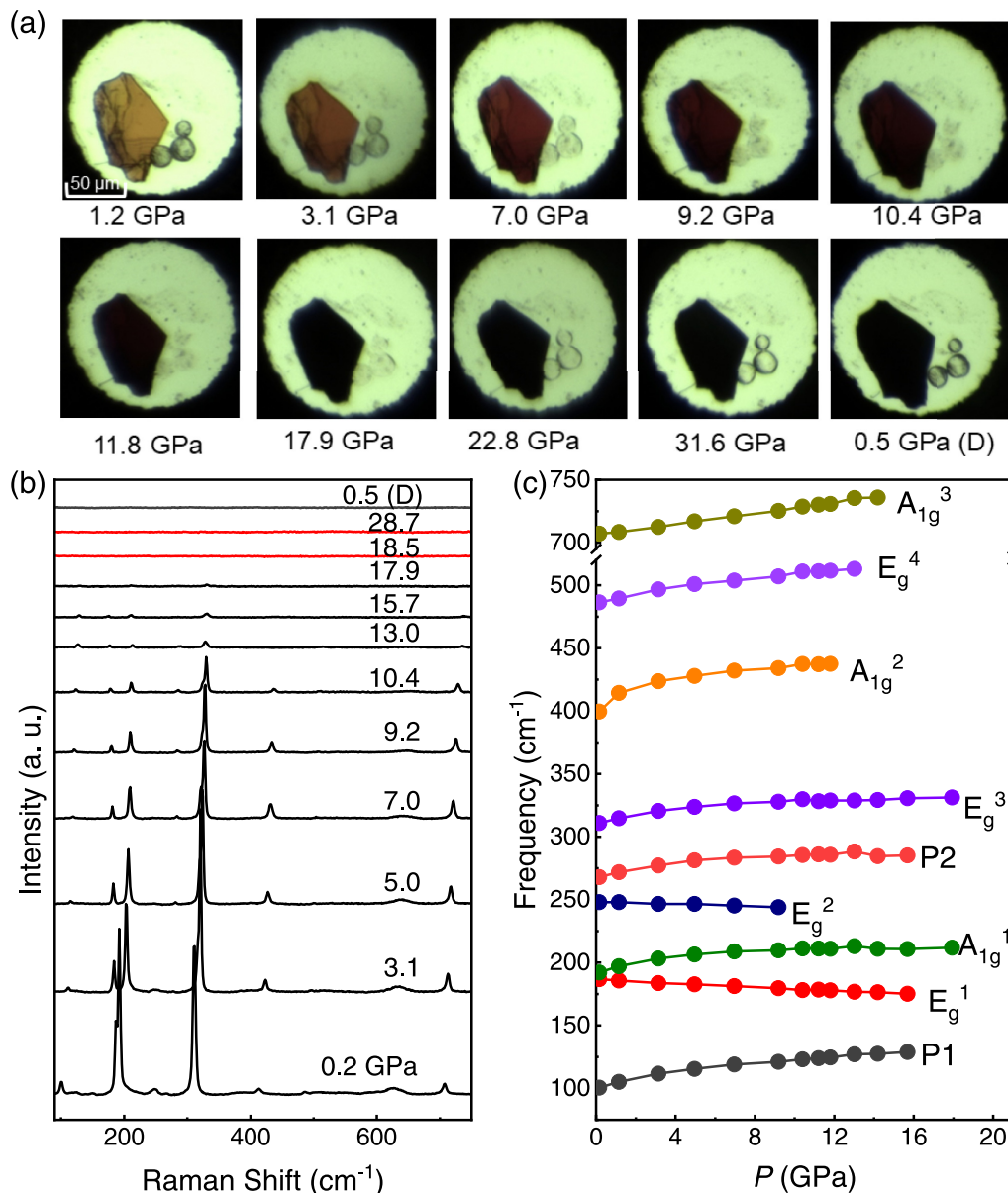


FIG. 4. (a) Optical micrographs of the Pd<sub>3</sub>P<sub>2</sub>S<sub>8</sub> single crystal collected at different pressures. The last one, 0.5 GPa (D), is for a state after decompression. (b) Raman spectra of the Pd<sub>3</sub>P<sub>2</sub>S<sub>8</sub> single crystal for different pressures, which are collected at room temperature with a laser wavelength of  $\lambda = 532$  nm. (c) Pressure-dependent frequencies of the detected Raman modes.

such kinds of unusual redshifts can be related to structural instability [38–40]. According to previous theoretical and experimental studies, the Raman modes  $E_g^1$  and  $E_g^2$  in Pd<sub>3</sub>P<sub>2</sub>S<sub>8</sub> are respectively associated with the bending and tilting vibrations of the tetrahedral [PS<sub>4</sub>]<sup>3-</sup> units [15]. The redshifts of modes  $E_g^1$  and  $E_g^2$  here may imply a structural instability of the [PS<sub>4</sub>]<sup>3-</sup> tetrahedrons under pressure. In support of this implication, the calculation results of Wang *et al.* [28] evidenced a transition of the coordination field of Pd from the original planar tetragonal field to a distorted octahedral one due to the enhanced coupling between interlayer Pd and S atoms upon compression. The amorphous phase may result from a transient of a structural transition into another crystalline phase, which cannot form properly due to kinetic barriers [41].

All the results are summarized in a phase diagram in Fig. 5. The intensity of a representative Raman mode  $E_g^3$  is also included. As is shown earlier, the XRD results evidence an amorphization of the system at  $\sim 20$  GPa. Here the pressure dependence of the Raman intensity, which displays a sharp drop at  $\sim 11$  GPa, indicates that the amorphous phase may already begin to form at this early pressure. Accompanied by the beginning of amorphization, metallization and onset superconducting transition are immediately observed. When the pressure is raised to  $\sim 20$  GPa, where the amorphization completes, a zero-resistance state is detected and, simultaneously, the Raman intensity vanishes. Therefore, the emergence of superconductivity is attributed to the formation of an amorphous phase. Moreover, XRD and Raman results consistently indicated that the crystal structure cannot be recovered

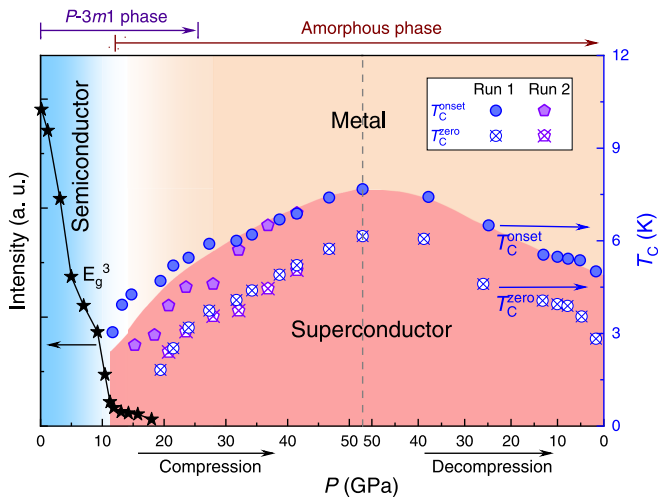


FIG. 5. The phase diagram of  $\text{Pd}_3\text{P}_2\text{S}_8$  as a function of pressure. The left axis stands for the Raman intensity of a representative mode  $E_g^3$ . The right axis corresponds to the superconducting critical temperatures  $T_c^{\text{onset}}$  and  $T_c^{\text{zero}}$ . The colored areas are guides to the eyes, indicating the distinct conducting phases of semiconductor, metal, and superconductor.

after the pressure is released, which therefore explains the retainability of superconductivity upon decompression.

#### IV. CONCLUSION

In summary, we have grown kagome single-crystal  $\text{Pd}_3\text{P}_2\text{S}_8$  and investigated the high-pressure electrical

transport and structural properties. We find that a pressure of  $\sim 11$  GPa induces a metallization and superconductivity in  $\text{Pd}_3\text{P}_2\text{S}_8$ . With increasing pressure, superconducting  $T_c$  continuously increases. Structural analyses show that the occurrence of superconductivity is due to the formation of an amorphous phase. As a result of the irreversible nature of the amorphization, superconductivity can be preserved to ambient conditions.

#### ACKNOWLEDGMENTS

This work was financially supported by the National Key Research and Development Program of China (Grant No. 2018YFA0305704), the National Natural Science Foundation of China (Grants No. 12204004, No. 11874362, No. U1932152, No. 12174395, No. U19A2093, and No. 12004004), the Natural Science Foundation of Anhui Province (Grants No. 2008085QA40 and No. 1908085QA18), the Key Project of Natural Scientific Research of Universities in Anhui Province (Grants No. KJ2021A0068 and No. KJ2021A0064), the Users with Excellence Project of Hefei Center CAS (Grants No. 2021HSC-UE008 and No. 2020HSC-UE015), and the Collaborative Innovation Program of Hefei Science Center, CAS (Grant No. 2020HSC-CIP014). A portion of this work was supported by the High Magnetic Field Laboratory of Anhui Province under Contract No. AHHM-FX-2020-02. Y. H. Z. was supported by the Youth Innovation Promotion Association CAS (Grant No. 2020443). The x-ray diffraction experiment was performed at the beamline BL15U1, Shanghai Synchrotron Radiation Facility.

- [1] I. I. Mazin, H. O. Jeschke, F. Lechermann, H. Lee, M. Fink, R. Thomale, and R. Valentí, *Nat. Commun.* **5**, 4261 (2014).
- [2] J.-W. Rhim and B.-J. Yang, *Adv. Phys.: X* **6**, 1901606 (2021).
- [3] H. Zhao, H. Li, B. R. Ortiz, S. M. L. Teicher, T. Park, M. Ye, Z. Wang, L. Balents, S. D. Wilson, and I. Zeljkovic, *Nature (London)* **599**, 216 (2021).
- [4] S. Cho, H. Ma, W. Xia, Y. Yang, Z. Liu, Z. Huang, Z. Jiang, X. Lu, J. Liu, Z. Liu, J. Li, J. Wang, Y. Liu, J. Jia, Y. Guo, J. Liu, and D. Shen, *Phys. Rev. Lett.* **127**, 236401 (2021).
- [5] B. R. Ortiz, S. M. L. Teicher, Y. Hu, J. L. Zuo, P. M. Sarte, E. C. Schueller, A. M. M. Abeykoon, M. J. Krogstad, S. Rosenkranz, R. Osborn, R. Seshadri, L. Balents, J. He, and S. D. Wilson, *Phys. Rev. Lett.* **125**, 247002 (2020).
- [6] E. Liu *et al.*, *Nat. Phys.* **14**, 1125 (2018).
- [7] M. R. Norman, *Rev. Mod. Phys.* **88**, 041002 (2016).
- [8] D. F. Liu, A. J. Liang, E. K. Liu, Q. N. Xu, Y. W. Li, C. Chen, D. Pei, W. J. Shi, S. K. Mo, P. Dudin, T. Kim, C. Cacho, G. Li, Y. Sun, L. X. Yang, Z. K. Liu, S. S. P. Parkin, C. Felser, and Y. L. Chen, *Science* **365**, 1282 (2019).
- [9] E. W. Huang, M.-S. Vaezi, Z. Nussinov, and A. Vaezi, *Phys. Rev. B* **99**, 235128 (2019).
- [10] K. Matsumoto, D. Ogura, and K. Kuroki, *Phys. Rev. B* **97**, 014516 (2018).
- [11] K. Kuroki, T. Higashida, and R. Arita, *Phys. Rev. B* **72**, 212509 (2005).
- [12] N. Verma, T. Hazra, and M. Randeria, *Proc. Natl. Acad. Sci. USA* **118**, e2106744118 (2021).
- [13] S. Sayyad, E. W. Huang, M. Kitatani, M.-S. Vaezi, Z. Nussinov, A. Vaezi, and H. Aoki, *Phys. Rev. B* **101**, 014501 (2020).
- [14] S. Miyahara, S. Kusuta, and N. Furukawa, *Physica C* **460–462**, 1145 (2007).
- [15] B. Wu, R. Kempt, E. Kovalska, J. Luxa, A. Kuc, T. Heine, and Z. Sofer, *ACS Appl. Nano Mater.* **4**, 441 (2021).
- [16] P. K. Roy, P. Marvan, V. Mazánek, N. Antonatos, D. Bouša, E. Kovalska, D. Sedmidubský, and Z. Sofer, *ACS Appl. Mater. Interfaces* **13**, 30806 (2021).
- [17] X. Zhang *et al.*, *Nat. Catal.* **1**, 460 (2018).
- [18] C. Tang, C. Zhang, S. K. Matta, Y. Jiao, K. Ostrikov, T. Liao, L. Kou, and A. Du, *J. Phys. Chem. C* **122**, 21927 (2018).
- [19] Y. Jing and T. Heine, *J. Mater. Chem. A* **6**, 23495 (2018).
- [20] S. Yan, B.-C. Gong, L. Wang, J. Wu, Q. Yin, X. Cao, X. Zhang, X. Liu, Z.-Y. Lu, K. Liu, and H. Lei, *Phys. Rev. B* **105**, 155115 (2022).
- [21] S. Park, S. Kang, H. Kim, K. H. Lee, P. Kim, S. Sim, N. Lee, B. Karuppanan, J. Kim, J. Kim, K. I. Sim, M. J. Coak, Y. Noda, C. H. Park, J. H. Kim, and J. G. Park, *Sci. Rep.* **10**, 20998 (2020).
- [22] Y. Zhou, X. L. Chen, C. An, Y. H. Zhou, L. S. Ling, J. Y. Yang, C. H. Chen, L. L. Zhang, M. L. Tian, Z. T. Zhang, and Z. R. Yang, *Phys. Rev. B* **99**, 054501 (2019).

- [23] H. K. Mao, J. Xu, and P. M. Bell, *J. Geophys. Res.* **91**, 4673 (1986).
- [24] See Supplemental Material at <http://link.aps.org/supplemental/10.1103/PhysRevB.106.104512> for sample characterization at ambient pressure and some supporting data under pressure, which include Refs. [15,20,21,25,26].
- [25] C. Calareso, V. Grasso, and L. Silipigni, *Phys. Rev. B* **60**, 2333 (1999).
- [26] G. J. Piermarini, S. Block, and J. D. Barnett, *J. Appl. Phys.* **44**, 5377 (1973).
- [27] N. R. Werthamer, E. Helfand, and P. C. Hohenberg, *Phys. Rev.* **147**, 295 (1966).
- [28] Q. Wang, X. Qiu, C. Pei, B. Gong, L. Gao, Y. Zhao, W. Cao, C. Li, S. Zhu, M. Zhang, Y. Chen, K. Liu, and Y. Qi, [arXiv:2204.05179](https://arxiv.org/abs/2204.05179).
- [29] C. Suryanarayana and M. G. Norton, *X-Ray Diffraction* (Springer, New York, 1998).
- [30] S. H. Tolbert and A. P. Alivisatos, *Science* **265**, 373 (1994).
- [31] J.-Y. Chen, C.-S. Yoo, W. J. Evans, H.-P. Liermann, H. Cynn, M. Kim, and Z. Jenei, *Phys. Rev. B* **90**, 144104 (2014).
- [32] G. W. Lee, W. J. Evans, and C.-S. Yoo, *Proc. Natl. Acad. Sci. USA* **104**, 9178 (2007).
- [33] F. Birch, *Phys. Rev.* **71**, 809 (1947).
- [34] I. Efthimiopoulos, Z. T. Y. Liu, M. Kucway, S. V. Khare, P. Sarin, V. Tsurkan, A. Loidl, and Y. Wang, *Phys. Rev. B* **94**, 174106 (2016).
- [35] I. Efthimiopoulos, A. Yaresko, V. Tsurkan, J. Deisenhofer, A. Loidl, C. Park, and Y. Wang, *Appl. Phys. Lett.* **103**, 201908 (2013).
- [36] A. F. Goncharov and V. V. Struzhkin, *J. Raman Spectrosc.* **34**, 532 (2003).
- [37] A. A. Abrikovsov and V. M. Genkin, *Zh. Eksp. Teor. Fiz.* **65**, 842 (1973) [*Sov. Phys. JETP* **38**, 417 (1974)].
- [38] C. An, Y. Zhou, C. Chen, F. Fei, F. Song, C. Park, J. Zhou, H.-G. Rubahn, V. V. Moshchalkov, X. Chen, G. Zhang, and Z. Yang, *Adv. Mater.* **32**, 2002352 (2020).
- [39] T. Kume, T. Hiraoka, Y. Ohya, S. Sasaki, and H. Shimizu, *Phys. Rev. Lett.* **94**, 065506 (2005).
- [40] W. Cochran, *Phys. Rev. Lett.* **3**, 412 (1959).
- [41] A. K. Arora, *Solid State Commun.* **115**, 665 (2000).